

# PCCP

Accepted Manuscript



This is an *Accepted Manuscript*, which has been through the Royal Society of Chemistry peer review process and has been accepted for publication.

*Accepted Manuscripts* are published online shortly after acceptance, before technical editing, formatting and proof reading. Using this free service, authors can make their results available to the community, in citable form, before we publish the edited article. We will replace this *Accepted Manuscript* with the edited and formatted *Advance Article* as soon as it is available.

You can find more information about *Accepted Manuscripts* in the [Information for Authors](#).

Please note that technical editing may introduce minor changes to the text and/or graphics, which may alter content. The journal's standard [Terms & Conditions](#) and the [Ethical guidelines](#) still apply. In no event shall the Royal Society of Chemistry be held responsible for any errors or omissions in this *Accepted Manuscript* or any consequences arising from the use of any information it contains.

# New insights into the by-product fatigue mechanism of the photo-induced ring-opening in diarylethenes<sup>†</sup>

David Mendive-Tapia,<sup>\*a,b</sup> Aurélie Perrier,<sup>c</sup> Michael J. Bearpark,<sup>d</sup> Michael A. Robb,<sup>d</sup> Benjamin Lasorne,<sup>e</sup> and Denis Jacquemin<sup>\*a,f</sup>

Received Xth XXXXXXXXXX 20XX, Accepted Xth XXXXXXXXXX 20XX

First published on the web Xth XXXXXXXXXX 200X

DOI: 10.1039/b000000x

The photochromic properties of diarylethenes, one of the most studied class of molecular switches, are known to be controlled by non-adiabatic decay at a conical intersection seam. Nevertheless, as their fatigue-reaction mechanism – leading to non-photochromic products – is yet to be understood, we investigate the photo-chemical formation of the so-called by-product isomer using three complementary computational methods (MMVB, CASSCF and CASPT2) on three model systems of increasing complexity. We show that for the ring-opening reaction a transition state on  $S_1(2A)$  involving bond breaking of the penta-ring leads to a low energy  $S_1(2A)/S_0(1A)$  conical intersection seam, which lies above one of the transition states leading to the by-product isomer on the ground state. Therefore, radiationless decay and subsequent side-product formation can take place explaining the photo-degradation responsible for the by-product generation in diarylethene-type molecules. The effect of dynamical correlation and the possible role of inter-system crossing along the penta-ring opening coordinate are discussed as well.

## 1 Introduction

Photochromism is the reversible light-induced interconversion of a single chemical species between two or more isomers having different absorption spectra. Typical examples include fulgides, azobenzenes, spiropyrans and diarylethenes.<sup>1</sup> The latter family provides large contrasts between the two isomers and has thus attracted an increasing attention in recent years due to potential practical applications such as data storage devices,<sup>2</sup> molecular switches,<sup>3</sup> molecular machines<sup>4</sup> or molecular sensors.<sup>5</sup>

Ideally photochromic reactions are fully reversible, thus

they can be carried out virtually an infinite number of times. Nevertheless, irradiation may induce side-reactions leading to the formation of undesired products. This phenomenon, usually referred to as fatigue, has a great importance since it will limit the maximum number of cycles that the photo-conversion can be performed and consequently the life-time of the related devices. In this work we explore the fatigue mechanism leading to the so-called “diatropic” by-product<sup>6</sup> in diarylethenes by presenting a mechanism based upon a study of both the ground and first excited state Potential Energy Surfaces (PESs) topology. *We show that a transition state on the covalent excited state  $S_1(2A)$  controls the accessibility to a low energy  $S_1(2A)/S_0(1A)$  conical intersection seam, which eventually leads to the formation of the by-product isomer on the ground state.*

### 1.1 Experimental review

In spite of diarylethenes being in general strongly fatigue-resistant, it has been reported experimentally that some variants with thiophene rings cease to be photo-active due to the formation of two different side-products.<sup>6,7</sup> In this work we study the case of 1,2-bis(2-methyl-5-phenyl-3-thienyl)perfluorocyclopentene (Monomer in Figure 1), which leads to the formation a photo-stable violet by-product after 200 cycles coinciding with a decrease of the yield of the opening isomer, which suggests that this side-product is formed from the closed-ring isomer.

<sup>†</sup> Electronic Supplementary Information (ESI) available: Optimised geometries and CASPT2 energies. See DOI: 10.1039/b000000x/

<sup>a</sup> Chimie Et Interdisciplinarité, Synthèse, Analyse, Modélisation (CEISAM), UMR CNRS no. 6230, BP 92208, Université de Nantes, 2, Rue de la Houssinière, 44322 Nantes, Cedex 3, France. E-mail: denis.jacquemin@univ-nantes.fr, david.mendive@univ-nantes.fr.

<sup>b</sup> Research visitor, Department of Chemistry, Imperial College London, London SW7 2AZ, United Kingdom.

<sup>c</sup> Laboratoire Interfaces, Traitements, Organisation et Dynamique des Systèmes (ITODYS), CNRS UMR 7086, Université Paris 7 - Paris Diderot, Bâtiment Lavoisier, 15 rue Jean Antoine de Baïf, 75205 Paris Cedex 13, France.

<sup>d</sup> Department of Chemistry, Imperial College London, London SW7 2AZ, United Kingdom.

<sup>e</sup> Institut Charles Gerhardt Montpellier, UMR 5253, CNRS-UM2-ENSCM-UM1, CTMM, Université Montpellier 2, CC 1501, Place Eugène Bataillon, 34095 Montpellier, France.

<sup>f</sup> Institut Universitaire de France, 103, blvd Saint-Michel, F-75005 Paris Cedex 05, France.

A more puzzling case occurs when two 1,2-dithienylethene photochromes are covalently joined forming a photochromic dyad (Dimer in Figure 1).<sup>8</sup> Experimentally, UV irradiation of the open-open isomer leads to the formation of the mono-cyclized closed-open isomer very efficiently. However, further irradiation does not result in the expected cyclization of the second unit to form the closed-closed dyad. Instead, a by-product-open dimer is formed derived from the previously closed diarylethene unit.

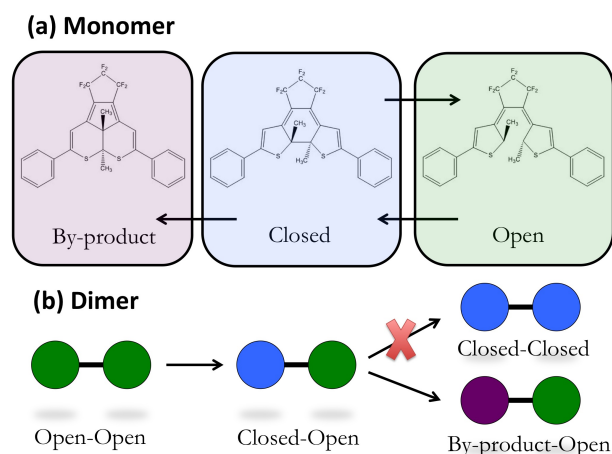


**Fig. 1** Experimental formation of the by-product isomer in diarylethenes. Two cases: a) Monomer: photochromic interconversion between closed and open forms, leads to the formation a photo-stable violet by-product and b) Dimer: irradiation of the open-open isomer leads to the formation of the closed-open isomer. However, further irradiation does not result in the expected closed-closed since the by-product-open dyad is formed instead.

## 1.2 Theoretical review

The experimental evidence described above suggests that, upon excitation of closed-ring diarylethenes, there is a subtle balance between adiabatic reactivity and non-adiabatic decay processes, yielding to either the closed (CHD, cf. cyclohexadiene), open (HT, cf. hexatriene) or by-product (BP) ground state products.<sup>‡</sup> Therefore, in the following we give a brief outline of the central theoretical and conceptual features of the photo-chemical mechanism in diarylethenes. The aim is to summarise these essential concepts before presenting our results in detail.

**1.2.1 Model systems.** In order to describe the smallest experimental target system, 1,2-bis(2-methyl-5-phenyl-3-thienyl)perfluorocyclopentene (Monomer in Figure 1) at the Complete Active Space Self-Consistent Field (CASSCF)

level, the obvious choice would be an active space consisting of 22 electrons in 22 molecular orbitals, e.g. CAS(22,22). Computations on such an active space are not feasible. Thus, Model I in Figure 2, a smaller but closely related model system, has been the object of numerous theoretical studies.<sup>9–12</sup>

Here we focus on three complementary model systems of increasing complexity (Models II–IV), which are shown in Figure 2. Model II includes the rigidity derived from incorporating the central double bond into a cyclopentene bridge, while Model III adds the effect of the sulphur heteroatoms. As we show in Section 3.2 by comparing Model II and Model III, the presence of the sulphur heteroatoms on the penta-ring does not change the main mechanistic features at a qualitative level. Finally, Model IV (without sulphur heteroatoms) is the closest to the experimentally studied photochrome (Monomer in Figure 1).

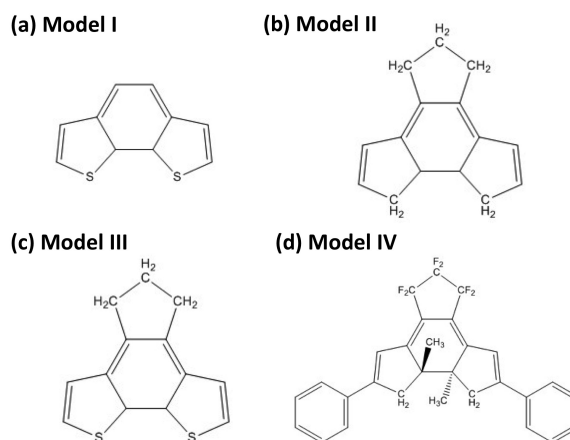


**Fig. 2** Model systems in diarylethenes. Model systems I and II are the simplest cases; in the first, one can evaluate the effect of the sulphur heteroatoms, while in the second the effect of the rigid cyclopentene bridge. Model system III contains both aspects. Model system IV is the closest to the experimental target system.

**1.2.2 Ground state reactivity.** In terms of mechanistic information about the formation of the BP isomer only the ground state has to the best of our knowledge been documented.<sup>13</sup> It is therefore convenient to begin with a brief description of the ground state PES topology as a prelude to the discussion of the photo-chemical reactivity.

The main transition states and minima leading from the CHD to the BP isomers for Model I–III are given in Figure 3. The first point to notice is that, from the CHD isomer, the process is triggered by the dissociation of one of the two C-CH<sub>2</sub> or C-S bonds. This leads to the formation of two intermediates, which eventually form the BP. Second, in the region of the C-CH<sub>2</sub> or C-S dissociation we find two stationary points (TS<sub>2</sub> and Planar Minimum (PM)), which span a high-energy

<sup>‡</sup> Due to their resemblance to cyclohexadiene and hexatriene, closed-ring and open-ring isomers are denoted as CHD and HT, respectively.

region. As shown in Section 3.1, radiationless decay in this region via a conical intersection seam may develop into either the regeneration of the CHD isomer or the formation of the BP.

It must be noted that the  $TS_1$  and  $TS_2$  barriers are considerably small (14.1 and 7.0 kcal/mol at the RHF/6-31++G(3df,3pd) level of theory) from the PM intermediate side. When comparing with ref. [13], methyl and benzene substitution causes the vanishing of the PM intermediate, thus the  $TS_2$  directly connects the CHD and bicyclohexane (BCH) ground state minima. This substitution dependency in the ground state mechanism for the formation of the BP isomer does not affect the general conclusion of this study. As we show in Section 3, the key element of the photo-chemical side-product formation is the non-adiabatic decay at the high energy dissociation region, which can be spanned either by  $TS_2$  or by both,  $TS_2$  and PM, depending on the details of the molecular structure of the considered diarylethene and possibly the level of theory employed.

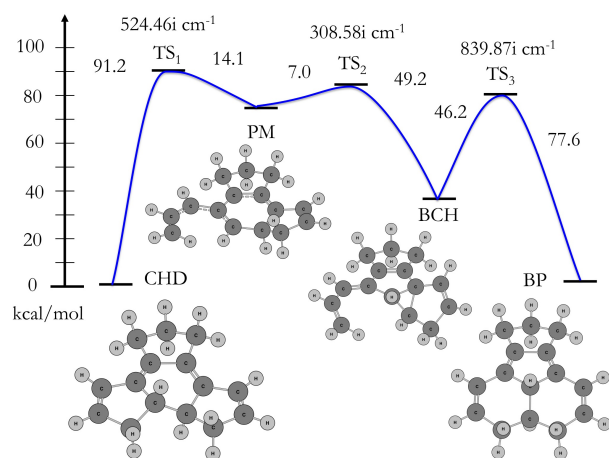


**Fig. 3** Ground state mechanism for the formation of the BP from the CHD isomer in Model II at the RHF/6-31++G(3df,3pd) level of theory. See ESI for a detailed view of the optimised structures.

**1.2.3 First excited state reactivity.** Previous studies have not addressed the photo-chemical formation of the BP isomer in diarylethenes. Nonetheless, the excited state mechanism of the ring-opening and ring-closing reactions has been theoretically studied in detail using semi-empirical,<sup>9</sup> and the CASSCF<sup>10–12</sup> method in Model I (Figure 1) as well as CASPT2 (complete active space second-order perturbation theory) energy evaluations performed on CASSCF optimised geometries<sup>14</sup> in Model III (Figure 1).

For the CHD and HT isomers, under  $C_2$  symmetry  $S_1(1B)$  and  $S_2(2A)$  are the two lowest electronic excited states in the Franck-Condon (FC) region.<sup>§</sup> The ionic  $S_1(1B)$  state is op-

tically active, whereas the covalent  $S_2(2A)$  is a dark state as shown by TD-DFT calculations on Model I,<sup>11</sup> and CASPT2//CASSCF computations on Model III<sup>14</sup>.

The analysis of Minimum Energy Paths (MEPs) from the FC and Conical Intersection (CI) geometries in Model I at the CASSCF level suggests that the system relaxes from the FC structure to the CHD\* minimum on the 1B PES.<sup>12</sup> Then, by continuing the geometrical change and with some excess of energy, the system can reach a CHD 1B/2A CI point, where efficient decay to 2A becomes possible. Although several processes can take place starting from this CHD 1B/2A CI point, all of the MEPs examined on the branching plane led exclusively to the CHD\* minimum on the 2A PES. Furthermore, the CHD\* minima on these two PESs, 2A and 1B, are very close in energy (1.1 kcal/mol energy difference) at the CASPT2//CASSCF level.<sup>12</sup>

Therefore, in the following we concentrate on the behaviour of the covalent  $S_1(2A)$  state, since according to previous studies the photochemical transformations in diarylethenes most likely occur on this PES. As MEPs at the CASSCF level suggest and considering that the  $S_1(1B)$  and  $S_1(2A)$  CHD\* minima are very close in energy, we can assume that rapid radiationless decay in the FC region from 1B to 2A and equilibration towards the  $S_1(2A)$  CHD\* minimum occurs soon after initial vertical excitation.

Figure 4 shows an illustration of the known photo-mechanism in diarylethene photochromism. The potential energies for the  $S_0(1A)$  (orange, bottom) and  $S_1(2A)$  (green, top) electronic states are represented in the space of two nuclear coordinates. These two independent coordinates correspond to: 1) the internuclear C-C distance connecting CHD and HT isomers (reaction coordinate) and 2) a linear combination of the Gradient Difference Vector (GDV) and Derivative Coupling Vector (DCV) that lift the degeneracy at the conical intersection labeled as ConInt<sub>1</sub> (branching space coordinate).

As described in ref. [11], the origin of the photochromic properties in diarylethenes is the presence and accessibility of ConInt<sub>1</sub> and its branching space being orthogonal to the opening/closing reaction coordinate.

On the one hand, for the ring-closing reaction, the system decays to  $S_0(1A)$  at the ConInt<sub>1</sub> before finding the barrier formed by  $TS_5$  (shown in Figure 4). This mechanism, suggested by the computation of non-adiabatic molecular dynamics simulations,<sup>11</sup> explains the highly effective and ultra-fast ring-closure.

On the other hand, the ring-opening reaction encounters a barrier on  $S_1(2A)$  before reaching the same seam of degeneracy, which accounts for temperature dependence and the usually lower ring-opening Quantum Yield (QY) observed experimentally compared to the ring-closure reaction. This “bot-

tomice we also use the 1A, 2A and 1B notation for all the model systems.

§ Strictly speaking, only Model I has  $C_2$  symmetry. Nevertheless, for conve-

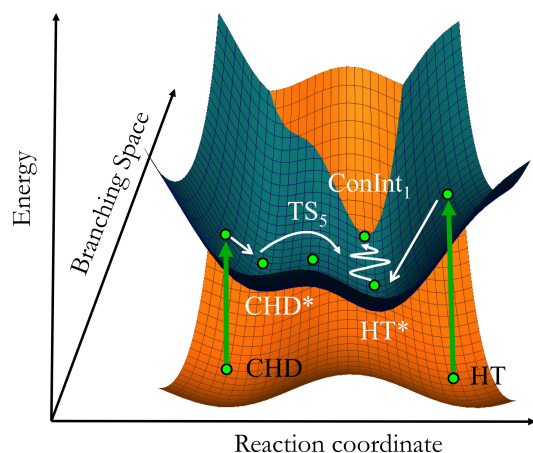


**Fig. 4** Sketch of the known mechanism in diarylethene photochromism. The energies for the  $S_0(1A)$  (orange, bottom) and  $S_1(2A)$  (green, top) electronic states are represented in the space of two nuclear coordinates: 1) the internuclear C-C distance connecting CHD and HT isomers (reaction coordinate) and 2) a linear combination of the DCV and GDV defined at the  $\text{ConInt}_1$  geometry (branching space coordinate).

tleneck” at the  $S_1(2A)$   $\text{CHD}^*$  minimum on the covalent dark state is also consistent with the reported correlation between experimental QYs and the energy difference on the  $S_1(2A)$  PES between the  $\text{CHD}^*$  and  $\text{HT}^*$  isomers when varying the structure by chemical substitution on the diarylethene core.<sup>10</sup> If the system inevitably decays and equilibrates at the  $S_1(2A)$   $\text{CHD}^*$  minimum, then the adiabatic reactivity on this PES (TS barriers between  $\text{CHD}^*$  and  $\text{HT}^*$  isomers and between  $\text{CHD}^*$  and other isomers, i.e. the BP) is what controls the efficiency of the ring-opening reaction.

## 2 Computational details

First we notice that the central objective of this work is to gain mechanistic information, thus we do not attempt to make quantitative predictions (i.e. attempting to compute reaction QYs). Here, we aim for a description of the topology of the PESs (existence of minima, TSs and CI surface crossings) at a qualitative level.

### 2.1 CASSCF

The most critical decision in CASSCF computations is the choice of the active space. In our calculations we used CAS(10,10) and CAS(12,12) active spaces consisting of eight  $\pi, \pi^*$  orbitals plus two or four  $\sigma, \sigma^*$  orbitals, respectively. In the first case describing one and in the second both of the  $\sigma$  bonds that are formed/broken (e.g. CHD/HT interconversion or C-CH<sub>2</sub>/C-S bond breaking) for modelling Model

II and Model III (Figure 2). As we show in Section 3.2, CAS(14,12) calculations including the lone pairs of the sulphur heteroatoms in the active space for Model III does not lead to significant changes.

Stationary points were optimised at the CASSCF level without imposing any symmetry constraint and numerical frequency calculations were used in all of our computations to ascertain the nature of the stationary points. Transition states were optimised using a starting Hessian partially computed numerically along the reaction coordinate, as analytical second derivatives are not feasible with such large active spaces. Conical intersections were optimised using the standard algorithm in Gaussian 09.<sup>15</sup> When state-averaged orbitals were used the orbital rotation derivative contribution from the CP-MCSCF equations to the gradient (which is usually a small correction and zero at a intersection seam geometry) was neglected. All CASSCF calculations were performed in a standard 6-31G(d) Pople basis set and with the Gaussian 09 quantum chemistry package.<sup>16</sup>

### 2.2 MMVB

The Molecular Mechanics Valence Bond (MMVB) hybrid method<sup>17</sup> uses a parameterised Heisenberg Hamiltonian<sup>18</sup> to simulate CASSCF active orbitals in a valence bond space and the molecular mechanics MM2 force field<sup>19</sup> to describe an inert molecular  $\sigma$  framework. For a full description of MMVB we refer to previous works.<sup>17,20,21</sup>

In short, the molecular system is divided into two parts: one to be treated by Valence Bond (VB) theory and the other to be treated by Molecular Mechanics (MM). VB wave functions can be written as eigenfunctions of what is known as the Heisenberg spin Hamiltonian. The parameters of this Hamiltonian have a simple physical interpretation as Coulomb and exchange integrals and they are molecule and state independent. In the MMVB method these have been parameterised from small CASSCF model calculations. The result is a parameterised VB Hamiltonian from *ab initio* data, which has already been used in diarylethene-type molecules<sup>11</sup> and in a number of other examples,<sup>22–24</sup> reproducing CASSCF geometries and energies for covalent states.

The main advantage of the MMVB method is that provides a description of excited states in large conjugated systems that takes into account static correlation. Nevertheless, an important drawback is that it can be used for a limited number of problems since the VB part has only been parameterised for  $sp^2$  and  $sp^3$  carbon atoms and for covalent, but not ionic states.<sup>25</sup> For the MM part any type of atoms can be included within the standard MM2 force field. All MMVB calculations were performed with a development version of the Gaussian 09 program.<sup>26</sup>

### 2.3 CASPT2

To account for dynamical electronic correlation, CASPT2 calculations were carried out by using the MOLCAS 7.8 software.<sup>27</sup> For each optimised geometry, three-root state-averaged calculations with equal weight were performed at the CASSCF/6-31G(d) level of theory and were followed by single root CASPT2/6-31G(d) calculations relying on the SA-CASSCF wavefunctions. These were performed using a CAS(10,10) active space including 8  $\pi, \pi^*$  and the  $\sigma, \sigma^*$  orbitals from the bond that was formed/broken, e.g. the C-CH<sub>2</sub> or the C-S bond. During the CASPT2 calculations, an imaginary shift of 0.1 a.u. was applied to avoid the effects of intruder states while losing only a minimal amount of dynamical correlation energy.

## 3 Results and discussion

This section is divided into three subsections 3.1-3.3. First, we discuss the structures and the reaction pathways on S<sub>1</sub>(2A) that are relevant for the BP fatigue mechanism in Model II at CASSCF level. Following this, in the next subsection we justify the choice of this model system by showing that the S<sub>1</sub>(2A) PESs of Model II and Model III have the same topology using CASSCF. Therefore, inclusion or not of the sulphur does not change the qualitative description of the PES. Finally, we conclude by applying the MMVB approach to the much larger Model IV in order to show that an approximated nevertheless calibrated description can be obtained for realistic molecules. These results confirm the same mechanistic picture in the experimental target system without sulphur heteroatoms, in which full active space CASSCF computations are not feasible.

### 3.1 By-product fatigue mechanism

We focus our discussion around the sketch shown in Figure 5, in which the potential energies for the S<sub>0</sub>(1A) (orange, bottom) and S<sub>1</sub>(2A) (green, top) electronic states are represented in the space of two nuclear coordinates. These two independent coordinates correspond to: 1) as in Figure 4, the internuclear C-C distance connecting CHD and HT isomers (reaction coordinate) and 2) the internuclear C-CH<sub>2</sub> distance, which triggers the BP formation (initial fatigue coordinate).

Two minima (corresponding to CHD\* and HT\* isomers) and two transition states (TS<sub>4</sub> and TS<sub>5</sub>) were located on the S<sub>1</sub>(2A) PES. The first transition state (labelled as TS<sub>4</sub> in Figure 5) describes the bond-breaking of the C-CH<sub>2</sub> bond of the penta-ring. The second is the asymmetric transition structure connecting CHD\* and HT\* (labelled as TS<sub>5</sub> in Figure 4 and Figure 5) accounting for the adiabatic excited state photochromic reaction and in agreement with ref. [11] (see the

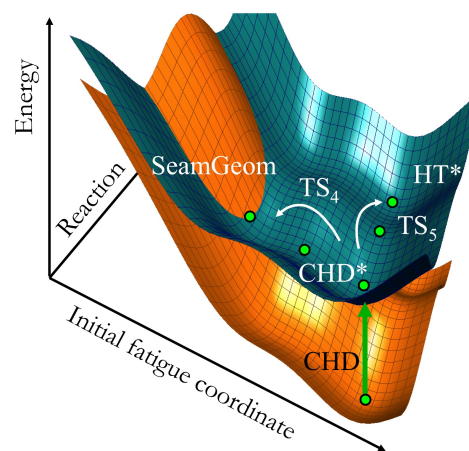


**Fig. 5** Sketch of the BP fatigue mechanism in diarylethene photochromism. The energies for the S<sub>0</sub>(1A) (orange, bottom) and S<sub>1</sub>(2A) (green, top) electronic states are represented in the space of two nuclear coordinates: 1) the internuclear C-C distance connecting CHD and HT isomers (reaction coordinate) and 2) the internuclear C-CH<sub>2</sub> distance (initial fatigue coordinate).

ESI).

An Internal Reaction Coordinate (IRC) computation was performed from TS<sub>4</sub>. In the reverse direction it terminated in the CHD\* S<sub>1</sub>(2A) minimum and in the forward direction it terminated in a S<sub>1</sub>(2A)/S<sub>0</sub>(1A) conical intersection seam geometry (labelled as SeamGeom). The optimised geometry of the lowest energy point on this conical intersection seam (labelled as ConInt<sub>2</sub>) is shown in Figure 6 and differs from the last point of the IRC (SeamGeom) mainly in the C-CH<sub>2</sub> distance, which is much longer, and that it is located 31.4 kcal/mol below at the CAS(10,10)/6-31G(d) level. These structures are shown in Figure 6, while the respective energies are collected in Table 1.

**Table 1** CASSCF and CASPT2 energies for Model II at the optimised geometries on the S<sub>1</sub>(2A) PES. Energies are in kcal/mol and with the CHD\* 2A minimum as reference. For CASPT2 energy evaluations the energy difference between the 2A and 1B electronic states are given in brackets. Energies at intersection seam geometries are state-averaged.

Structure	CAS(10,10)	CAS(12,12)	CASPT2
CHD*	0.0	0.0	0.0 (30.3)
HT*	11.7	11.9	–
TS <sub>4</sub>	43.7	43.8	44.3 (11.8)
TS <sub>5</sub>	17.0	16.4	–
ConInt <sub>1</sub>	32.2	33.4	–
ConInt <sub>2</sub>	-18.3	-17.0	-9.7 (50.7)
SeamGeom	13.1	13.2	–

The IRC calculated from TS<sub>4</sub> in Model II does not actually

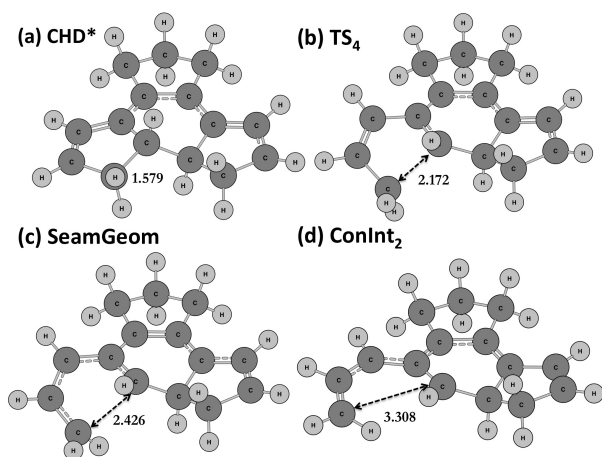


**Fig. 6** Optimised structures on the  $S_1(2A)$  PES of Model II at the CAS(12,12)/6-31G(d) level. C-CH<sub>2</sub> bond distances are in angstroms.

reach the ConInt<sub>2</sub> itself, the lowest-energy point found on the intersection space. We can understand this by comparing the DCV and GDV at the optimised ConInt<sub>2</sub> geometry with the transition vector at TS<sub>4</sub> (Figure 7). The branching space vectors are the directions that lift the degeneracy up to first order. Therefore, as these vectors are dominated by in-plane distortions and do not involve the formation/breaking of the C-CH<sub>2</sub>  $\sigma$  bond, one expects the crossing to persist for a wide range of values along the C-CH<sub>2</sub> bond distance coordinate including the structure SeamGeom. One could say that the transition vector is approximately orthogonal to the branching space and thus a coordinate along which the intersection seam of degeneracy can be spanned.

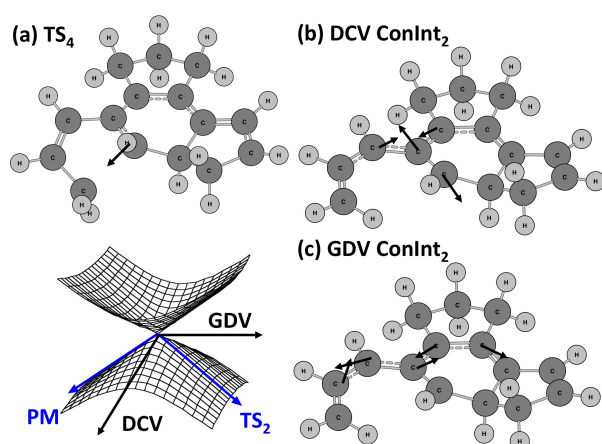


**Fig. 7** Optimised TS<sub>4</sub> on  $S_1(2A)$  and ConInt<sub>2</sub> of Model II at the CAS(12,12)/6-31G(d) level. The transition vector and branching space are shown for each case respectively.

According to the sketch illustrated in Figure 5 and derived from these CASSCF computations, we would expect that after non-adiabatic decay from 1B to 2A the system will evolve on the  $S_1(2A)$  PES until reaching the  $S_1(2A)$  CHD\* minimum. Then, after equilibration, two outcomes can be expected: 1) the system can cross the TS<sub>5</sub> barrier (17.0 kcal/mol at the CAS(10,10)/6-31G(d) level) to reach the flat HT plateau, or 2) the system can cross the TS<sub>4</sub> barrier (43.7 kcal/mol at the CAS(10,10)/6-31G(d) level) via bond breaking of one of the five-member ring, provided there is sufficient energy in the C-CH<sub>2</sub> dissociation coordinate.

To establish the products that can be formed after decay, ground state optimisations were run after distortion along the GDV at ConInt<sub>2</sub>. These indicated the presence of two distinct pathways, one leading to the ground state PM minima and the other to the transition state TS<sub>2</sub> in Figure 3. At which geometry the system will decay, ConInt<sub>2</sub> or SeamGeom, will depend on the details of the dynamics something which is outside the scope of the present work. Nevertheless, once the C-CH<sub>2</sub>  $\sigma$  bond is broken beyond the TS<sub>4</sub> geometry on  $S_1(2A)$ , we expect that the inertia will keep this bond length increasing at the crossing and lead mostly to the BP rather than back to the  $S_0(1A)$  CHD minimum on the ground state.

### 3.2 Justifying Model II and Model III

The effect of including the sulphur heteroatoms and their respective lone pairs in the CASSCF computations was tested. Geometry optimisations were carried out for the  $S_1(2A)$  state at the CHD\* minimum, TS<sub>4</sub> and ConInt<sub>2</sub> geometries for Model III, with 14 electrons in 12 orbitals including the lone pairs from one of the sulphur atoms. The structures and energies for the first excited state  $S_1(2A)$  are given in Figure 8 and Table 2, respectively.

As can be seen, there are no significant differences from the corresponding structures for Model II discussed in Section 3.1. In terms of energies, the TS<sub>4</sub> barrier was found to be 19.9 and 31.9 kcal/mol lower in energy than for model II with a CAS(10,10) and a CAS(14,12) active space, respectively. This suggests that the sulphur substitution somehow facilitates the fatigue mechanism going from Model II to Model III. Due to the main critical points were located for Model II and III and as the differences in energy are not significant, we conclude that the PESs for both systems possess qualitatively the same topology.

Next, we discuss the effect of adding dynamical correlation to the previous CASSCF results. Previous studies,<sup>12,14</sup> have shown that the inclusion of dynamic correlation stabilises the 1B state, making this state lower than the 2A in the FC geometry. In order to evaluate this effect along the bond breaking of the penta-ring, we computed CASPT2 energy evaluations at the CASSCF relevant geometries (CHD\*, TS<sub>4</sub> and ConInt<sub>2</sub>)

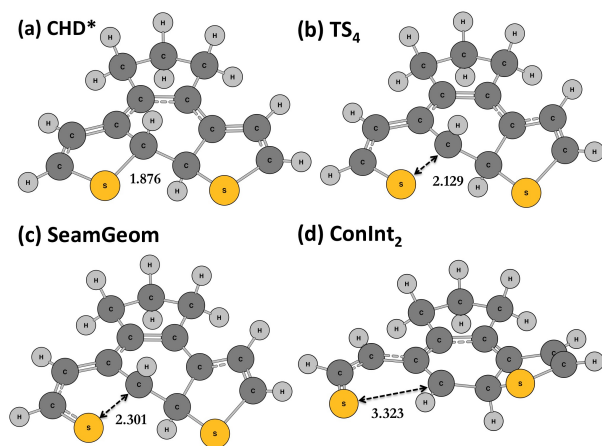


**Fig. 8** Optimised structures on the  $S_1(2A)$  PES of Model III at the CAS(14,12)/6-31G(d) level. C-S distances are in angstroms.

**Table 2** CASSCF and CASPT2 energies for Model III at the optimised geometries on the  $S_1(2A)$  PES. Energies are in kcal/mol and with the CHD\*  $S_1$  minimum as reference. For CASPT2 energy evaluations the energy difference between the 2A and 1B electronic states are given in brackets. Energies at conical intersection geometries are state-averaged.

Structure	CAS(10,10)	CAS(14,12)	CASPT2
CHD*	0.0	0.0	0.0 (33.6)
HT*	5.90	4.2	–
TS <sub>4</sub>	22.6	10.0	8.5 (22.1)
TS <sub>5</sub>	10.1	7.7	–
ConInt <sub>1</sub>	39.6	36.9	–
ConInt <sub>2</sub>	-21.3	-20.1	-9.4 (7.4)
SeamGeom	–	5.2	–

for Model II and Model III. Inversion of the electronic state ordering was not observed except for the ConInt<sub>2</sub> geometry in which the 1B state became 7.4 kcal/mol lower than the 1A/2A degeneracy (see Tables 1, 2 and the ESI).

These CASPT2//CASSCF results confirm the existence of the ConInt<sub>2</sub> degeneracy (0.73 and 0.07 kcal/mol energy gap for Models II and III respectively) and that the 1B state still is above the 2A state at the TS<sub>4</sub> geometry (11.8 and 22.1 kcal/mol for Models II and III respectively) when adding dynamical correlation for both systems (see Tables 1, 2 and the ESI). In contrast with the CASSCF picture, the 1B state seems to be stabilised when the penta-ring is fully opened. Nevertheless, in order to properly check the state ordering at the ConInt<sub>2</sub> degeneracy, one should ideally carry out a geometry optimisation at the CASPT2 level. Unfortunately, this computational strategy is still out of reach for the systems under study.

Last, the possible role played by triplet electronic states in the non-radiative decay of Model III should be briefly ad-

ressed. At the TS<sub>4</sub> geometry the  $S_1$  and  $T_1$  electronic states in Model III are almost degenerate (3.0 kcal/mol energy difference) and exhibit a moderate spin-orbit coupling (18  $\text{cm}^{-1}$ ) at the CAS(10,10)/6-31G(d) level, which could lead to an ultrafast inter-system crossing. This effect completely vanishes when comparing to Model II, which proves that this change is due to the presence of sulphur heteroatoms. Therefore, an inter-system crossing mechanism might compete with the singlet state decay mechanism described here when including sulphur heteroatoms. For instance, ultrafast time-scales for inter-system crossing capable of competition with internal conversion have been reported in other organic molecules even with a small (order of a few  $\text{cm}^{-1}$ ) spin orbit coupling.<sup>28,29</sup>

Nevertheless, even though theoretical analysis of the singlet and triplet PESs in thiophene suggest the competition between singlet and triplet states along the C-S dissociation coordinate in order to explain the ultrafast radiationless decay from the first excited state,<sup>30,31</sup> more recent studies including analysis of PESs and mixed quantum-classical dynamics also suggest that this inter-system crossing is a minor pathway and that photo-excited thiophene decays primarily via its singlet electronic states.<sup>31–33</sup> Therefore, according to the aforementioned work on thiophene, even though possible such alternative inter-system crossing decay pathway seems more likely to be minor in comparison with the singlet mechanism.

### 3.3 MMVB force field picture

The aim of this final section is to apply the MMVB approach to Model IV, for which full active space computations, e.g. CAS(22,22) are not feasible. In quantum chemistry, a problem is often studied using a hierarchy of increasingly accurate (and costly) methods to try to obtain the necessary accuracy with a minimum cost. From this ideal, comes the concept of the *Model Chemistries*,<sup>34</sup> which Ernest R. Davidson refers to as “calibrated *ab initio*”.<sup>35</sup> In practical computations, however, one does not routinely carry out theoretical calculations using the most accurate method available (e.g. Full Configuration Interaction (FCI)). Instead it is usually preferable to apply approximate, but well-calibrated methodologies across a range of chemical systems.

Figure 9 shows the optimised structures for Model IV using MMVB. The respective energies are given in Table 3 together with the MMVB energies and CAS(12,12) results previously discussed for Model II. Bond lengths for Model II are within 0.05 angstroms on average of the values obtained with CAS(12,12). Energy barriers, which are much larger than at the CASSCF level, are less satisfactory. As in ref. [11] this inaccuracy is explained due to our current parameterisation of the terms in the Heisenberg Hamiltonian needed to describe the  $\sigma$ -bond breaking/formation. As a consequence, CHD structures (with the new  $\sigma$ -bond) are systematically much

lower in energy relative to HT structures in comparison with CASSCF. Nevertheless, at a qualitative level both MMVB and CASSCF yield the same picture, especially for  $TS_4$ , in which the quantitative agreement is better (20.2 kcal/mol energy difference).

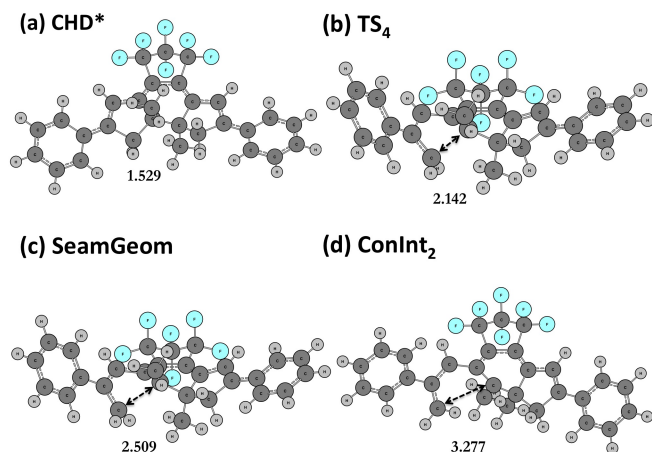


**Fig. 9** Optimised structures on the  $S_1(2A)$  PES of Model IV at the MMVB level. C-CH<sub>2</sub> bond distances are in angstroms.

After showing that the MMVB topology is a reasonable qualitative approximation to CASSCF in diarylethenes, we discuss the change going from Model II to Model IV at the MMVB level. The  $TS_4$  for Model IV is very similar to the Model II (bond lengths match within 0.025 angstroms) and the associated transition vector is also very similar. The main difference is a considerable increase in the  $TS_4$  energy barrier, which would hinder the BP fatigue mechanism. This makes sense from an experimental point of view, as benzene substituents are commonly used in diarylethene-type switches.<sup>3</sup> Nevertheless, as we pointed out earlier, one should take with care any MMVB energetics as there is a systematic tendency to yield over-stabilised CHD structures.

In short, we conclude that MMVB correctly describes the geometries and the nature of the main stationary points for Model II and predicts the qualitative preservation of the same fatigue mechanism for the experimental target Model IV.

## 4 Conclusions

In this paper we have focused our attention on the photo-fatigue mechanism responsible for the formation of the so-called BP isomer in diarylethenes. The three theoretical methods (MMVB, CASSCF and CASPT2) used on three different model systems (Models II-IV), predict the existence of a transition state on the  $S_1(2A)$  electronic state, which leads to an accessible  $S_1(2A)/S_0(1A)$  conical intersection seam. A

**Table 3** CASSCF(12,12)/631G(d) energies for Model II and MMVB energies for Model II and Model III at the optimised geometries on the  $S_1(2A)$  PES. Energies are in kcal/mol and with the CHD\* 2A minimum as reference. CASSCF energies at conical intersection geometries are state-averaged.

Structure	CAS(12,12)	MMVB Model II	MMVB Model IV
CHD*	0.0	0.0	0.0
$TS_4$	43.8	64.0	93.0
$TS_5$	16.4	75.9	-
ConInt <sub>2</sub>	-17.0	38.8	88.8

new relaxation decay pathway described for the first time to our knowledge, which lies above the ground state mechanism leading to the formation of the BP isomer.

Approximate MMVB calculations on the experimental target system Model IV corroborate the same insightful picture previously found on the smaller Model II and Model III systems at the more accurate CASSCF level of theory. This Model IV lacks the presence of sulphur atoms on the pentaring CH<sub>2</sub> positions since the MMVB approach has been parameterised only for carbon atoms. Nevertheless, via comparison of Model II and Model III we have shown that this does not change the qualitative topology of the PESs (existence of minima, TSs and CI surface crossings). This mechanism, which proceeds in three steps, is schematically represented in Figure 10:

1. First, after vertical excitation in the FC region, internal conversion between 1B and 2A leads to the CHD\* minimum on the  $S_1(2A)$  PES. This step consists mainly in the change of the distribution of the conjugation in the eight  $\pi$  carbon atoms.
2. Second, the C-CH<sub>2</sub> or C-S bond increases leading to the  $TS_4$ . The details of the molecular structure, e.g. substituents, will control the efficiency of the process as a function of the adiabatic reactivity. The available kinetic energy will determine if it is possible to overcome the barrier (depending of the energy accumulated after relaxation from FC and temperature) and the value of the barrier itself in comparison to the barrier leading to the photochromic decay mechanism (dependent on the energy barriers when comparing  $TS_4$  and  $TS_5$  in Figure 5). For instance, this is 43.7 and 17.0 kcal/mol for Model II at the CAS(10,10)/6-31G(d) level and 10.8 and 7.7 kcal/mol for Model III at the CAS(14,12)/6-31G(d) level.
3. The third step consists in the non-adiabatic decay at the conical intersection seam directly connected to  $TS_4$ . As previously said, at which geometry the system will decay, SeamGeom or ConInt<sub>2</sub>, will depend on the details of the dynamics. Nonetheless, we expect that in a dynamics

trajectory the inertia will keep the C-CH<sub>2</sub> or C-S  $\sigma$  bond length increasing at the crossing and lead mostly to the BP rather than back to the CHD minimum on the ground state in Figure 3. A final system-dependent factor that would affect the decay geometry is the energy gap along the IRC reaction coordinate and the shape of the conical intersection seam.<sup>36</sup>

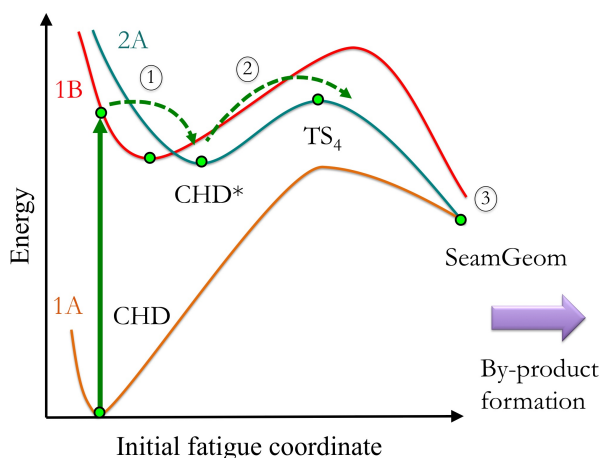


**Fig. 10** Sketch of the initial BP fatigue mechanism in diarylethenes after vertical excitation in the FC region.

The existence of such radiationless decay path offers a rationalisation for the photo-degradation responsible of the BP generation in diarylethene-type molecules and plausible explanations for several experimental observations. For example, UV irradiation of the closed-ring isomer causes the BP formation, while visible irradiation does not.<sup>7,37</sup> This could be explained as a shorter wavelength promotes the system to higher excited states providing an excess of kinetic energy that helps the “hot” molecule to overcome the fatigue barrier. Furthermore, group substitution in diarylethenes strongly affects their photochromism and fatigue properties.<sup>6,38–40</sup> The particular case of methyl substitution at the 4 and 4' positions might be explained due to the steric repulsion between the methyl groups, the cyclopentene bridge and the phenyl substituents, which would obstruct the C-S bond breaking. Last, the BP formation has been shown to be suppressed in solid state,<sup>41,42</sup> which might be explained also through a steric effect induced by the crystalline packing.

We do not discard the possibility that the C-CH<sub>2</sub> or C-S bond breaking, which triggers the process, may occur on the 1B PES before non-adiabatic decay to 2A. Reactivity on an ionic excited state has been observed in other photochromic systems, furyl fulgides.<sup>43</sup> Nevertheless, this would not affect the conclusions of this work since it would establish a complementary pathway leading to the BP isomer. However, confirmation of this conjecture would become a very challenging

task since accurate description of the 2B ionic state requires the inclusion of both static and dynamical correlation.

Finally, from the computation of the spin-orbit coupling at the TS<sub>4</sub> optimised geometry for Model III, intersystem crossing is conceivable as an alternative radiationless decay path and as a possible precursor for the BP formation. To our knowledge this is the first time that inter-system crossing has been suggested to have a relevant role in diarylethene photochromism. Further insights require an extended analysis of the triplet PESs, while efficiency comparison and discrimination between both possible mechanistic pathways would require time-dependent dynamical simulations besides quantum chemistry calculations. These are highly desirable studies that we hope will be addressed in future works.

## 5 Acknowledgements

D. M. T. thanks Agisilaos Chantzis for helpful discussions in this work and the European Research Council (ERC, Marches - 278845) for his post-doctoral funding. D. J. acknowledges the European Research Council (ERC) and the *Région des Pays de la Loire* for financial support in the framework of a Starting Grant (Marches – 278845) and a *recrutement sur poste stratégique*, respectively. This research used resources of: 1) the GENCI-CINES/IDRIS (Grants c2013085117), 2) CCIPL (*Centre de Calcul Intensif des Pays de Loire*), 3) a local Troy cluster and 4) the Imperial College London High Performance Computing Service for the MMVB computations.

## References

- 1 V. Balzani, M. Venturi and A. Credi, *Molecular Devices and Machines: A Journey into the Nanoworld*, Wiley, 2006.
- 2 K. Uno, H. Niikura, M. Morimoto, Y. Ishibashi, H. Miyasaka and M. Irie, *J. Am. Chem. Soc.*, 2011, **133**, 13558–13564.
- 3 M. Irie, *Chem. Rev.*, 2000, **100**, 1685–1716.
- 4 M. Morimoto and M. Irie, *J. Am. Chem. Soc.*, 2010, **132**, 14172–14178.
- 5 C. Yun, J. You, J. Kim, J. Huh and E. Kim, *J. Photochem. Photobiol. C*, 2009, **10**, 111 – 129.
- 6 M. Irie, T. Lifka, K. Uchida, S. Kobatake and Y. Shindo, *Chem. Commun.*, 1999, 747–750.
- 7 K. Higashiguchi, K. Matsuda, T. Yamada, T. Kawai and M. Irie, *Chem. Lett.*, 2000, **29**, 1358–1359.
- 8 A. Peters and N. R. Branda, *Adv. Mater. Opt. Electron.*, 2000, **10**, 245–249.
- 9 J. Ern, A. Bens, H.-D. Martin, S. Mukamel, D. Schmid, S. Tretiak, E. Tsiper and C. Kryschi, *Chem. Phys.*, 1999, **246**, 115 – 125.
- 10 D. Guillaumont, T. Kobayashi, K. Kanda, H. Miyasaka, K. Uchida, S. Kobatake, K. Shibata, S. Nakamura and M. Irie, *J. Phys. Chem. A*, 2002, **106**, 7222–7227.
- 11 M. Boggio-Pasqua, M. Ravaglia, M. J. Bearpark, M. Garavelli and M. A. Robb, *J. Phys. Chem. A*, 2003, **107**, 11139–11152.
- 12 Y. Asano, A. Murakami, T. Kobayashi, A. Goldberg, D. Guillaumont, S. Yabushita, M. Irie and S. Nakamura, *J. Am. Chem. Soc.*, 2004, **126**, 12112–12120.

- 13 P. D. Patel, I. A. Mikhailov, K. D. Belfield and A. E. Masunov, *Int. J. Quantum Chem.*, 2009, **109**, 3711–3722.
- 14 A. Perrier, S. Aloise, M. Olivucci and D. Jacquemin, *J. Phys. Chem. Lett.*, 2013, **4**, 2190–2196.
- 15 M. J. Bearpark, M. A. Robb and H. B. Schlegel, *Chem. Phys. Lett.*, 1994, **223**, 269 – 274.
- 16 M. J. Frisch, G. W. Trucks, H. B. Schlegel, G. E. Scuseria, M. A. Robb, J. R. Cheeseman, G. Scalmani, V. Barone, B. Mennucci, G. A. Petersson, H. Nakatsuji, M. Caricato, X. Li, H. P. Hratchian, A. F. Izmaylov, J. Bloino, G. Zheng, J. L. Sonnenberg, M. Hada, M. Ehara, K. Toyota, R. Fukuda, J. Hasegawa, M. Ishida, T. Nakajima, Y. Honda, O. Kitao, H. Nakai, T. Vreven, J. A. Montgomery, Jr., J. E. Peralta, F. Ogliaro, M. Bearpark, J. J. Heyd, E. Brothers, K. N. Kudin, V. N. Staroverov, R. Kobayashi, J. Normand, K. Raghavachari, A. Rendell, J. C. Burant, S. S. Iyengar, J. Tomasi, M. Cossi, N. Rega, J. M. Millam, M. Klene, J. E. Knox, J. B. Cross, V. Bakken, C. Adamo, J. Jaramillo, R. Gomperts, R. E. Stratmann, O. Yazyev, A. J. Austin, R. Cammi, C. Pomelli, J. W. Ochterski, R. L. Martin, K. Morokuma, V. G. Zakrzewski, G. A. Voth, P. Salvador, J. J. Dannenberg, S. Dapprich, A. D. Daniels, Ö. Farkas, J. B. Foresman, J. V. Ortiz, J. Cioslowski and D. J. Fox, *Gaussian 09, Revision B.01*, Gaussian Inc. Wallingford CT, 2010.
- 17 F. Bernardi, M. Olivucci and M. A. Robb, *J. Am. Chem. Soc.*, 1992, **114**, 1606–1616.
- 18 P. W. Anderson, *Phys. Rev.*, 1959, **115**, 2–13.
- 19 N. Allinger, *Adv. Phys. Org. Chem.*, 1976, **13**, 1 – 82.
- 20 M. J. Bearpark, F. Bernardi, M. Olivucci and M. A. Robb, *J. Phys. Chem. A*, 1997, **101**, 8395–8401.
- 21 M. J. Bearpark, M. A. Robb, F. Bernardi and M. Olivucci, *Chem. Phys. Lett.*, 1994, **217**, 513 – 519.
- 22 M. J. Bearpark, M. Boggio-Pasqua, M. A. Robb and F. Ogliaro, *Theor. Chem. Acc.*, 2006, **116**, 670–682.
- 23 G. Tomasello, F. Ogliaro, M. J. Bearpark, M. A. Robb and M. Garavelli, *J. Phys. Chem. A*, 2008, **112**, 10096–10107.
- 24 A. M. Tokmachev, M. Boggio-Pasqua, D. Mendive-Tapia, M. J. Bearpark and M. A. Robb, *J. Chem. Phys.*, 2010, **132**, 044306.
- 25 M. J. Bearpark, F. Ogliaro, T. Vreven, M. Boggio-Pasqua, M. J. Frisch, S. M. Larkin, M. Morrison and M. A. Robb, *J. Photochem. Photobiol. A*, 2007, **190**, 207 – 227.
- 26 M. J. Frisch, G. W. Trucks, H. B. Schlegel, G. E. Scuseria, M. A. Robb, J. R. Cheeseman, G. Scalmani, V. Barone, B. Mennucci, G. A. Petersson, H. Nakatsuji, M. Caricato, X. Li, H. P. Hratchian, A. F. Izmaylov, J. Bloino, G. Zheng, J. L. Sonnenberg, M. Hada, M. Ehara, K. Toyota, R. Fukuda, J. Hasegawa, M. Ishida, T. Nakajima, Y. Honda, O. Kitao, H. Nakai, T. Vreven, J. A. Montgomery, Jr., J. E. Peralta, F. Ogliaro, M. Bearpark, J. J. Heyd, E. Brothers, K. N. Kudin, V. N. Staroverov, R. Kobayashi, J. Normand, K. Raghavachari, A. Rendell, J. C. Burant, S. S. Iyengar, J. Tomasi, M. Cossi, N. Rega, J. M. Millam, M. Klene, J. E. Knox, J. B. Cross, V. Bakken, C. Adamo, J. Jaramillo, R. Gomperts, R. E. Stratmann, O. Yazyev, A. J. Austin, R. Cammi, C. Pomelli, J. W. Ochterski, R. L. Martin, K. Morokuma, V. G. Zakrzewski, G. A. Voth, P. Salvador, J. J. Dannenberg, S. Dapprich, A. D. Daniels, Ö. Farkas, J. B. Foresman, J. V. Ortiz, J. Cioslowski and D. J. Fox, *Gaussian Development Version, Revision H.13*, Gaussian Inc. Wallingford CT, 2010.
- 27 F. Aquilante, L. De Vico, N. Ferré, G. Ghigo, P. A. Malmqvist, T. B. Pedersen, M. Pitonak, M. Reiher, B. O. Roos, L. Serrano-Andrés, M. Urban, V. Veryazov and R. Lindh, *J. Comput. Chem.*, 2010, **31**, 224–247.
- 28 R. S. Minns, D. S. N. Parker, T. J. Penfold, G. A. Worth and H. H. Fielding, *Phys. Chem. Chem. Phys.*, 2010, **12**, 15607–15615.
- 29 M. Richter, P. Marquetand, J. González-Vázquez, I. Sola and L. González, *J. Phys. Chem. Lett.*, 2012, **3**, 3090–3095.
- 30 S. Salzmann, M. Kleinschmidt, J. Tatchen, R. Weinkauff and C. M. Marian, *Phys. Chem. Chem. Phys.*, 2008, **10**, 380–392.
- 31 M. Stenrup, *Chem. Phys.*, 2012, **397**, 18–25.
- 32 X.-F. Wu, X. Zheng, H.-G. Wang, Y.-Y. Zhao, X. Guan, D. L. Phillips, X. Chen and W. Fang, *J. Chem. Phys.*, 2010, **133**, 134507.
- 33 G. Cui and W. Fang, *J. Phys. Chem. A*, 2011, **115**, 11544–11550.
- 34 J. A. Pople, *Rev. Mod. Phys.*, 1999, **71**, 1267–1274.
- 35 E. R. Davidson, *Faraday Symp. Chem. Soc.*, 1984, **19**, 7–15.
- 36 J. J. Serrano-Pérez, F. de Vleeschouwer, F. de Proft, D. Mendive-Tapia, M. J. Bearpark and M. A. Robb, *J. Org. Chem.*, 2013, **78**, 1874–1886.
- 37 H. Jean-Ruel, R. R. Cooney, M. Gao, C. Lu, M. A. Kochman, C. A. Morrison and R. J. D. Miller, *J. Phys. Chem. A*, 2011, **115**, 13158–13168.
- 38 M. Irie, K. Sakemura, M. Okinaka and K. Uchida, *J. Org. Chem.*, 1995, **60**, 8305–8309.
- 39 K. Morimitsu, S. Kobatake, S. Nakamura and M. Irie, *Chem. Lett.*, 2003, **32**, 858–859.
- 40 Y.-C. Jeong, S. I. Yang, E. Kim and K.-H. Ahn, *Tetrahedron*, 2006, **62**, 5855 – 5861.
- 41 S. Kobatake and M. Irie, *Bull. Chem. Soc. Jpn.*, 2004, **77**, 195–210.
- 42 H. Jean-Ruel, M. Gao, M. A. Kochman, C. Lu, L. C. Liu, R. R. Cooney, C. A. Morrison and R. J. D. Miller, *J. Phys. Chem. B*, 2013, **117**, 15894–15902.
- 43 G. Tomasello, M. Bearpark, M. Robb, G. Orlandi and M. Garavelli, *Angew. Chem. Int. Ed.*, 2010, **49**, 2913–2916.